Astron. Astrophys. 359, 586–596 (2000)

ASTRONOMY AND ASTROPHYSICS

The $^{12}C/^{13}C$-ratio in cool carbon stars⋆

F.L. Schöier and H. Olofsson

Stockholm Observatory, 133 36 Saltsjöbaden, Sweden

Received 8 March 2000 / Accepted 8 May 2000

Abstract. We present observations of circumstellar millimetre-wave ^{13}CO line emission towards a sample of 20 cool carbon stars. Using a detailed radiative transfer model we estimate the circumstellar $^{12}CO/^{13}CO$-ratios, which we believe accurately measure the important stellar $^{12}C/^{13}C$-ratios. For those optically bright carbon stars where it is possible, our derived $^{12}C/^{13}C$-ratios are compared with the photospheric results, obtained with different methods. Our estimates agree well with those of Lambert et al. (1986).

It is shown that a straightforward determination of the $^{12}CO/^{13}CO$-ratio from observed line intensity ratios is often hampered by optical depth effects, and that a detailed radiative transfer analysis is needed in order to determine reliable isotope ratios.

Key words: stars: abundances – stars: AGB and post-AGB – stars: carbon – stars: circumstellar matter – stars: late-type

1. Introduction

The $^{12}C/^{13}C$-ratio is an important measure of stellar evolution and nucleosynthesis. Current theoretical models of stellar evolution on the asymptotic giant branch (AGB) predict that stars with "normal" chemical composition transform into carbon stars, from spectral type M via the intermediate states MS, S and SC, through the dredge-up of freshly synthesized carbon in He-shell flashes (Busso et al. 1999). This scenario is also confirmed by observations (Smith & Lambert 1985, 1990; Dominy et al. 1986; Lambert et al. 1986). Since mainly the ^{12}C-isotope is synthesized, there should be a coeval evolution in the $^{12}C/^{13}C$-ratio from the value determined during the first red giant evolution. In addition, processes like hot bottom burning will affect this ratio (Boothroyd et al. 1993), as well as set an upper mass limit for carbon stars. Thus, an accurate estimate of the $^{12}C/^{13}C$-ratio should increase our understanding of the processes that lead to the formation of carbon stars (e.g., Forestini & Charbonnel 1997; Wallerstein & Knapp 1998). The $^{12}C/^{13}C$-ratio is also an important tracer of the past starformation rate and stellar mass function (Prantzos et al. 1996; Greaves & Holland 1997).

In a classical paper, Lambert et al. (1986) determined the photospheric $^{12}C/^{13}C$-ratios of 30 optically bright carbon stars, by fitting stellar atmosphere models to near-IR data on the isotopomers of C_2, CO, and CN. A decade later Ohnaka & Tsuji (1996, 1999), based on a different method and data on the CN red system around 8000 Å, presented $^{12}C/^{13}C$-ratios that, on the average, are about a factor of two lower than those of Lambert et al. (1986) for the same stars. The activity in this field was further increased with the published results of Abia & Isern (1997). They derived $^{12}C/^{13}C$-ratios of 44 carbon stars, using the CN red system, which fell in between the results obtained by Lambert et al. (1986) and Ohnaka & Tsuji (1996). This is somewhat surprising since they used the same model atmospheres as Lambert et al. (1986), suggesting that the derived $^{12}C/^{13}C$-ratios depend on the spectral features used. It is difficult to identify the main reason for the different results obtained by Lambert et al. (1986) and Ohnaka & Tsuji (1996, 1999). The former used high-resolution near-infrared data, while the latter used data obtained closer to optical wavelengths. Also the atmospheric models differ. de Laverny & Gustafsson (1998) have investigated the method used by Ohnaka & Tsuji (1996) and found that it is very sensitive to model parameters and blends. Their conclusion is that the larger $^{12}C/^{13}C$-ratios determined by Lambert et al. (1986) are more reliable, since this analysis is rather insensitive to the adopted model parameters, and also the effect of blends is less severe, but the discussion continues (Ohnaka & Tsuji 1998; de Laverny & Gustafsson 1999). Recently, Ohnaka et al. (2000) have revised the values for three of the stars, which were originally published in Ohnaka & Tsuji (1996). Using new model atmospheres, they obtain $^{12}C/^{13}C$-ratios that are larger by about 40%, i.e., closer to those estimated by Lambert et al. (1986).

To shed light on this disturbing controversy, we have performed independent estimates of the $^{12}C/^{13}C$-ratio, using CO radio line emission from the circumstellar envelopes (CSEs), for a sample of carbon stars showing large discrepancies between the sets of photospheric estimates. Due to the weakness of the circumstellar ^{13}CO lines, and the difficulties in the interpretation of the circumstellar emission, only a few attempts have been made to determine the $^{12}CO/^{13}CO$ ratio in the CSEs of carbon stars (e.g., Knapp & Chang 1985; Sopka et al. 1989; Greaves & Holland 1997). In this paper we present new obser-

Send offprint requests to: F.L. Schöier (fredrik@astro.su.se)

⋆ Presented in this paper is observational data collected using the Swedish-ESO submillimetre telescope, La Silla, Chile, the 20 m telescope at Onsala Space Observatory, Chalmers Tekniska Högskola, Sweden, and the NRAO 12 m telescope located at Kitt Peak, USA.

Table 1. Source list

Source	α [B1950.0]	δ [B1950.0]	$^{12}C/^{13}C$ [1]	$^{12}C/^{13}C$ [2]
R Scl	01:24:40.0	−32:48:07	19	9
R Lep	04:57:19.6	−14:52:49	62	
W Ori	05:02:48.7	01:06:37	79	26
UU Aur	06:33:06.6	38:29:16	52	19
X Cnc	08:52:34.0	17:25:22	52	22
U Hya	10:35:05.1	−13:07:27	32	17
V Hya	10:49:11.3	−20:59:05	69	
Y CVn	12:42:47.1	45:42:48	3.5	2.0
RY Dra	12:54:28.2	66:15:53	3.6	1.9
T Lyr	18:30:36.1	36:57:38	3.2	
S Sct	18:47:37.1	−07:57:59	45	14
V Aql	19:01:44.0	−05:45:38	82	66
UX Dra	19:23:22.4	76:27:42	32	
AQ Sgr	19:31:27.1	−16:29:03	52	35
TX Psc	23:43:50.1	03:12:34	43	22

[1] Lambert et al. (1986); [2] Ohnaka & Tsuji (1996, 1999).

vational results, as well as a detailed modelling of circumstellar ^{12}CO and ^{13}CO radio line emission.

Table 2. Observational ^{13}CO results. A colon (:) marks an uncertain value due to a low signal to noise ratio (UU Aur) or contamination by interstellar lines (UX Dra).

Source	Tel.	Trans.	$T_{\rm mb}$ [K]	$I_{\rm mb}$ [K km s^{-1}]	v_* [km s^{-1}]	$v_{\rm e}$ [km s^{-1}]
R Scl	SEST	1−0	0.055	1.9	−19.0	15.1
	SEST	2−1	0.11	4.1	−19.0	15.2
R Lep	SEST	1−0		<0.20		
	SEST	2−1	0.015	0.47	10.1	16.7
W Ori	SEST	1−0		<0.18		
	SEST	2−1		<0.25		
UU Aur	OSO	1−0	0.016:	0.17:	8.4:	10.2:
X Cnc	SEST	1−0		<0.28		
	SEST	2−1		<0.27		
U Hya	SEST	2−1	0.066	0.77	−31.1	5.8
V Hya	SEST	1−0	0.031	0.67	−14.3	10.7
	SEST	2−1	0.032	1.1	−17.0	13.0
Y CVn	OSO	1−0	0.24	3.4	21.8	8.8
V Aql	SEST	1−0		<0.23		
	SEST	2−1		<0.29		
UX Dra	OSO	1−0	0.019:	0.14:	15.5:	4.5:
AQ Sgr	SEST	1−0		<0.12		
	SEST	2−1		<0.27		
TX Psc	SEST	1−0	0.009	0.12	13.5	8.1
	SEST	2−1	0.023	0.22	11.8	8.3

2. The observations

We have selected a sample of 11 optically bright carbon stars for which the photospheric $^{12}C/^{13}C$-ratios have been determined by Lambert et al. (1986) and Ohnaka & Tsuji (1996). This sample is presented in Table 1, where we have also included S Sct, which was observed by Bergman et al. (1993) and Olofsson el al. (1996), as well as the three J-type stars (i.e., stars with $^{12}C/^{13}C$-ratios $\sim$3) Y CVn, RY Dra, and T Lyr (see Table 4 for references). These 15 stars were also included in the major survey of circumstellar molecular line emission by Olofsson et al. (1993a,b).

The ^{13}CO observations were carried out in October 1998 using the Swedish-ESO submillimetre telescope (SEST) located on La Silla, Chile, and in March 1999 using the Onsala 20 m telescope (OSO), Sweden. At SEST, a dual channel, heterodyne SIS receiver was used to simultaneously observe at 110 GHz (the J=1→0 line) and 220 GHz (the J=2→1 line). The single sideband temperatures of the receiver are about 110 K and 150 K at 110 GHz and 220 GHz, respectively. All the available acousto-optical spectrometers were used as backends. The two wideband (1 GHz), low resolution spectrometers (LRSs) were used to cover both lines. The third, narrow band (86 MHz), high resolution spectrometer (HRS) was used at 220 GHz, since the J=2→1 line is usually stronger than the lowest rotational line in CSEs. The LRS had 1440 channels separated by 0.7 MHz whereas the HRS used 2000 channels separated by 42 kHz.

At OSO, an SIS receiver, with a single sideband temperature of about 100 K at 110 GHz, was used for the observations. As backends, two filterbanks with bandwidths of 512 MHz (MUL A) and 64 MHz (MUL B) were used. The MUL A used 512 channels separated by 1 MHz and the MUL B filterbank used 256 channels with a separation of 250 kHz.

The observations were made in a dual beamswitch mode, where the source is alternately placed in the signal and the reference beam, using a beam throw of about 12′ at SEST and about 11′ at OSO. This method produces two spectra that are subtracted from each other, which results in very flat baselines, i.e., most of the frequency dependant response of the system is removed. The intensity scales are given in main beam brightness temperature, $T_{\rm mb}$=$T_{\rm A}^{\star}/\eta_{\rm mb}$, where $T_{\rm A}^{\star}$ is the antenna temperature corrected for atmospheric attenuation using the chopper wheel method, and $\eta_{\rm mb}$ is the main beam efficiency. For the SEST $\eta_{\rm mb}$ is 0.7 at 110 GHz and 0.5 at 220 GHz. At OSO $\eta_{\rm mb}$=0.5 at 110 GHz. The beamsizes of the SEST are 45″ and 24″ at 110 GHz and 220 GHz, respectively. At OSO the beam is 34″ at 110 GHz. Regular pointing checks were made on strong SiO masers and the pointing was usually better than ±3″ for both telescopes. The uncertainty in the intensity scale is estimated to be about ±20%. The observational results are summarized in Table 2 and the detections of ^{13}CO line emission are shown in Fig. 1. These observations include first detections of circumstellar ^{13}CO emission towards R Lep, UU Aur, UX Dra, and TX Psc. The line parameters, i.e., the main beam brightness temperature at the line centre ($T_{\rm mb}$), the line centre velocity (v_*), and half the full line width ($v_{\rm e}$), are obtained by fitting the data with an artificial line profile (Olofsson et al. 1993a)

$$T(v) = T_{\rm mb}\left[1-\left(\frac{v-v_*}{v_{\rm e}}\right)^2\right]^{\gamma/2}, \quad (1)$$

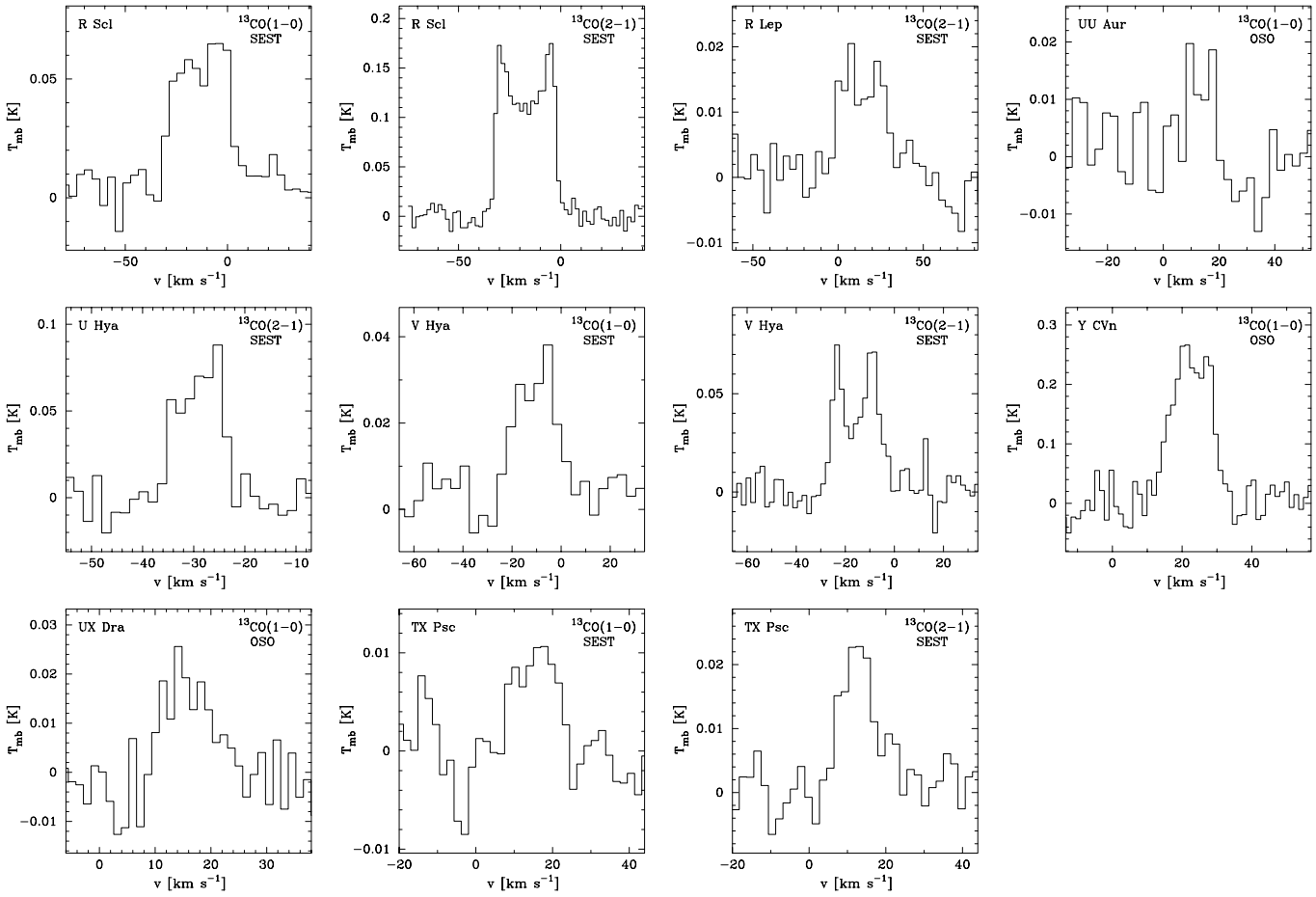

Fig. 1. New observations of circumstellar ^{13}CO line emission including first detections (see text for details). The line observed and the telescope used are shown in the upper right corner of each panel

where γ is a parameter describing the shape of the line. The integrated intensity ($I_{\rm mb}$) is obtained by integrating the emission between $v_*\pm v_{\rm e}$. The upper limits are obtained as $T_{\rm pp}2v_{\rm e}$, where $T_{\rm pp}$ is the peak-to-peak noise obtained from spectra where the velocity resolution has been degraded to twice the expansion velocity. The corresponding ^{12}CO lines were also observed, simultaneously with the ^{13}CO lines, for all the sample stars. Spectra of these lines have been published in Olofsson et al. (1993a).

To complement these new observations we have collected additional ^{13}CO data and, in particular, ^{12}CO data on the sample stars, as well as for an additional seven stars for comparison, from various sources and included them in the modelling (see Table 4).

3. Radiative transfer

In order to model the circumstellar line emission, and to determine accurate ^{12}CO/^{13}CO abundance ratios, we have used a non-LTE radiative transfer code based on the Monte Carlo method [see Schöier (2000) for details]. Assuming a spherically symmetric CSE expanding at a constant velocity, the code calculates the molecular excitation, i.e., the level populations, required to solve the radiative transfer exactly.

The excitation of the CO molecules were calculated taking into account 30 rotational levels in each of the ground and first vibrational states. The transition probabilities and energy levels are taken from Chandra et al. (1996), and the rotational collisional rate coefficients (CO-H_2) are based on the results in Flower & Launay (1985) (they are extrapolated for J>11 and for temperatures higher than 250 K). Collisional transitions between vibrational levels are not important due to low densities and short radiative lifetimes.

The basic physical parameters of the CSE, e.g., the mass loss rate, expansion velocity, and temperature structure, are determined from the analysis of the observed ^{12}CO radio line emission. CO is well suited for this purpose since it is difficult to photodissociate and easy to excite through collisions, and thus is a very good tracer of the molecular gas and its temperature. The kinetic temperature of the gas is derived in a self-consistent manner, i.e., the calculations include the most important heating and cooling mechanisms for the gas, e.g., heating due to dust-gas collisions and molecular line cooling from CO. Once the characteristics of the CSE have been determined, the ^{13}CO excitation analysis is performed. The ^{13}CO abundance is varied

Table 3. Input parameters and derived ^{12}CO/^{13}CO-ratios from the radiative transfer calculations. A colon (:) marks an uncertain ^{12}CO/^{13}CO-ratio estimate that is based on observations of only one ^{13}CO transition.

Source	D [pc]	L [$L_\odot$]	T_* [K]	$T_{\rm d}$ [K]	$L_{\rm d}/L_*$	$\dot{M}$ [$M_\odot$/yr]	$v_{\rm e}$ [km s^{-1}]	$r_{\rm p}$ [cm]	^{12}CO/^{13}CO	τ[^{12}CO(2→1)][b]
R Scl[a]	360[2]	5500	2000			4×10^{-6}	16.5	7.0×10^{16}	20	1.5
V384 Per	560[2]	8100	1900	890	10.0	3.5×10^{-6}	15.0	1.4×10^{17}	35	2.4
R Lep	250[1]	4000	1900	820	0.14	7×10^{-7}	18.0	5.3×10^{16}	90:	0.90
W Ori	220[1]	2600	2200			7×10^{-8}	11.0	1.9×10^{16}	>30	0.28
UU Aur	260[2]	6900	2500			3.5×10^{-7}	11.0	4.2×10^{16}	45:	1.1
X Cnc	280[2]	2800	2200			1.0×10^{-7}	7.0	2.4×10^{16}	>30	1.3
CW Leo	120[2]	9600		510		1.5×10^{-5}	14.5	3.7×10^{17}	50	5.4
RW LMi	440[2]	9700	1300	510	6.7	6×10^{-6}	17.0	1.9×10^{17}	35	1.7
U Hya	160[1]	2500	2400			1.4×10^{-7}	7.0	2.9×10^{16}	40	1.4
Y CVn	220[1]	4400	2200			1.5×10^{-7}	8.5	3.1×10^{16}	2.5	0.87
RY Dra	490[1]	10000	2500			3×10^{-7}	10.0	4.0×10^{16}	3.0:	0.40
IRAS 15194-5115	600[2]	8800	930	480	2.2	1.0×10^{-5}	21.5	3.2×10^{17}	5.5	1.4
T Lyr	340[3]	4000	2000			7×10^{-8}	11.5	1.8×10^{16}	3.0:	0.14
S Sct[a]	400[1]	4900	2400			4×10^{-5}	16.5	4.0×10^{17}	35:	0.90
V Aql	370[1]	6500	2100			3×10^{-7}	8.5	4.2×10^{16}	>70	1.4
UX Dra	310[3]	4000	2600			1.6×10^{-7}	4.0	4.0×10^{16}	25:	2.9
AQ Sgr	420[3]	4000	2700			2.5×10^{-7}	10.0	3.6×10^{16}	>40	0.93
V Cyg	370[2]	6200	1500	860	0.84	1.2×10^{-6}	11.5	8.5×10^{16}	20	1.1
RV Aqr	670[2]	6800	1300	620	0.46	2.5×10^{-6}	16.0	1.1×10^{17}	35:	1.5
LP And	630[2]	9400	1100	610	6.6	1.5×10^{-5}	14.0	4.0×10^{17}	55	7.3

[a] Detached CSE; [b] The maximum tangential optical depth in the ^{12}CO(J=2→1) derived from the model.
[1] Hipparcos; [2] Period-luminosity relation (Groenewegen & Whitelock 1996); [3] L=4000 $L_\odot$ assumed.

until a satisfactory fit to the observations is obtained. In this way the circumstellar ^{12}CO/^{13}CO-ratio is estimated.

The spatial extent of the molecular envelope is an important input parameter, and the derived mass loss rate and, to a lesser extent, the ^{12}CO/^{13}CO-ratio will depend on this. The size of the circumstellar CO envelope, assumed to be the same for ^{12}CO and ^{13}CO, was estimated based on the modelling presented in Mamon et al. (1988). It includes photodissociation, self-shielding and H_2-shielding, and chemical exchange reactions. Here we assume the radial fractional abundance distribution to follow

$$f(r) = f_0 \exp\left[-\ln 2 \left(\frac{r}{r_{\rm p}}\right)^{\alpha}\right], \quad (2)$$

where f_0 is the initial (photospheric) abundance with respect to H_2, $r_{\rm p}$ is the photodissociation radius (where the abundance has dropped to $f_0/2$), and α is a parameter describing the rate at which the abundance declines. Both $r_{\rm p}$ and α depend on the mass loss rate, the expansion velocity, and f_0. When modelling the ^{12}CO emission we assume f_0=1×10^{-3}. This is an average of the f_0:s estimated by Olofsson et al. (1993b) for a sample of optically bright carbon stars.

In our models we include both a central source of radiation and the cosmic background radiation at 2.7 K. The central radiation emanates from the star itself, which may be approximated by a blackbody. For heavily dust-enshrouded objects, like CW Leo (a.k.a. IRC+10216), most of the stellar light is re-emitted by dust at longer wavelenghts. This emission source is also approximated by a blackbody. For low mass loss rate objects, the stellar blackbody temperature, T_*, was estimated from a fit to the SED of the object. For stars of intermediate to high mass loss rates, two blackbodies were used, one representing the stellar contribution and one representing the dust. A fit to the SED gives the two blackbody temperatures, T_* and $T_{\rm d}$, and the relative luminosities of the two blackbodies, $L_{\rm d}/L_*$. The method is described in Kerschbaum (1999). The temperatures and luminosities used in the modelling are presented in Table 3. The inner boundary of the CSE was set to be outside the radius of the central blackbody(s), but never lower than 1×10^{14} cm.

The distances, presented in Table 3, were estimated using one of the following methods: the observed Hipparcos parallax, a period-luminosity relation (Groenewegen & Whitelock 1996), or an assumed bolometric luminosity. In the two former cases the luminosities were estimated using apparent bolometric magnitudes and the distances.

In the case of V Hya and TX Psc, stars with possible bipolar outflows (Heske et al. 1989; Kahane et al. 1996), no radiative transfer analysis was attempted due to the complexity of these outflows.

4. Model results

4.1. The ^{12}CO modelling

As explained above, the ^{12}CO line emission is used to derive the basic parameters of the CSE. The observational constraints for each source are presented in Table 4. The main part of the observational data used here are the J=1→0 and J=2→1 spec-

Table 4. CO modelling results compared with observations.

Source	Tel.	Trans.	^{12}CO			^{13}CO			$I(^{12}CO)/I(^{13}CO)$[a]
			I_{obs} [K km s^{-1}]	I_{mod} [K km s^{-1}]	Ref.	I_{obs} [K km s^{-1}]	I_{mod} [K km s^{-1}]	Ref.	
R Scl	SEST	1−0	26.1	29.6	4	1.9	2.3	1	12
	IRAM	1−0	76.2	79.2	4				
	SEST	2−1	47.8	49.8	4	4.2	4.0	1	10
	JCMT	2−1	50.6	54.8	7				
	IRAM	2−1	67.7	72.0	4				
	SEST	3−2	63.7	28.0	6				
	JCMT	3−2	62.9	30.5	7				
V384 Per	NRAO	1−0	7.8	10.1	2				
	OSO	1−0	25.5	25.1	4	2.1	2.1	5	11
	IRAM	1−0	52.7	48.4	4				
	JCMT	2−1	37.3	35.2	7				
	IRAM	2−1	83.6	102.0	4				
	JCMT	3−2	44.5	42.5	7	4.4	4.3	7	9
R Lep	SEST	1−0	6.2	6.7	4	<0.20	0.07	1	>33
	IRAM	1−0	31.7	24.3	4				
	SEST	2−1	18.1	17.4	4	0.5	0.5	1	31
	IRAM	2−1	56.4	64.2	4				
	SEST	3−2	12.5	21.6	2				
	JCMT	3−2	28.1	27.9	7				
W Ori	SEST	1−0	1.2	1.3	2	<0.18	0.02	1	>6
	OSO	1−0	2.7	2.4	4				
	IRAM	1−0	5.0	5.1	4				
	SEST	2−1	4.9	4.3	2	<0.25	0.25	1	>17
	IRAM	2−1	19.0	16.9	4				
	SEST	3−2	4.8	5.4	2				
UU Aur	OSO	1−0	7.9	8.2	4	0.17	0.17	1	40
	IRAM	1−0	18.8	16.9	4				
	JCMT	2−1	16.8	14.8	7				
	IRAM	2−1	39.0	46.2	4				
X Cnc	NRAO	1−0	0.7	0.7	2				
	SEST	1−0	1.5	1.1	2	<0.28	0.03	1	>5
	OSO	1−0	1.7	2.0	4				
	SEST	2−1	3.2	2.9	2	<0.27	0.27	1	>10
	IRAM	2−1	11.1	11.8	4				
CW Leo	NRAO	1−0	170.8	257.1	2	16.9	22.1	3	9
	SEST	1−0	288.1	305.3	4	24.3	26.8	5	11
	OSO	1−0	422.0	391.7	4	31.1	32.7	3	12
	SEST	2−1	487.3	580.5	4	64.9	73.9	3	7
	JCMT	2−1	731.8	632.2	7	76.9	79.9	7	8
	IRAM	2−1	1057.7	1116.1	4				
	SEST	3−2	854.8	774.0	2				
	JCMT	3−2	1066.3	883.7	7	157.3	130.4	7	6
	JCMT	4−3	1227.8	1052.0	7				
RW LMi	NRAO	1−0	36.4	37.0	2	2.4	2.4	3	13
	SEST	1−0	54.6	51.9	4				
	OSO	1−0	87.0	83.8	4	5.6	5.3	5	14
	SEST	2−1	105.4	128.4	4				
	JCMT	2−1	163.2	147.4	7	10.3	11.9	7	14
	JCMT	3−2	245.3	208.6	7	13.8	16.4	7	15
	JCMT	4−3	243.1	224.3	7				
U Hya	SEST	1−0	5.4	5.4	4	0.20	0.13	5	23
	SEST	2−1	13.8	14.1	4	0.8	1.0	1	15
	JCMT	2−1	20.2	16.6	7				
	IRAM	2−1	48.8	48.7	4				

Table 4. (continued)

Source	Tel.	Trans.	^{12}CO			^{13}CO			$I(^{12}CO)/I(^{13}CO)$[a]
			I_{obs} [K km s^{-1}]	I_{mod} [K km s^{-1}]	Ref.	I_{obs} [K km s^{-1}]	I_{mod} [K km s^{-1}]	Ref.	
Y CVn	NRAO	1−0				1.0	1.0	1	
	OSO	1−0	4.5	5.4	4	3.4	2.4	1	1.2
	IRAM	1−0	10.3	11.2	4				
	JCMT	2−1	11.9	10.9	7				
	IRAM	2−1	22.7	34.2	4				
	JCMT	3−2	20.9	15.6	7	7.9	7.7	7	2.3
RY Dra	OSO	1−0	2.4	3.0	4				
	IRAM	2−1	21.6	28.3	4				
	JCMT	3−2	18.9	15.8	7	5.8	5.4	7	2.8
IRAS 15194-5115	SEST	1−0	53.5	49.1	9	14.1	13.3	9	3.3
	SEST	2−1	114.0	111.2	9	30.5	32.8	9	3.3
	SEST	3−2	131.5	138.7	10				
T Lyr	OSO	1−0	0.7	1.0	4				
	IRAM	2−1	5.6	9.6	4				
	JCMT	3−2	6.4	4.3	7	1.8	2.0	7	3.1
S Sct	SEST	1−0	5.3	4.9	6	0.21	0.19	6	22
	IRAM	1−0	5.3	4.7	4				
	SEST	2−1	2.7	2.7	6				
	JCMT	2−1	2.4	2.8	7				
	IRAM	2−1	2.8	2.4	4				
	SEST	3−2	1.0	0.9	6				
	JCMT	3−2	1.0	0.9	7				
V Aql	SEST	1−0	2.8	2.6	4	<0.23	0.03	1	>11
	OSO	1−0	3.2	4.8	4				
	SEST	2−1	8.1	7.0	4	<0.29	0.28	1	>24
	JCMT	2−1	9.0	8.3	7				
	JCMT	3−2	11.2	10.6	7				
UX Dra	OSO	1−0	2.1	1.7	4	0.14	0.14	1	9
	IRAM	2−1	6.8	9.0	4				
AQ Sgr	SEST	1−0	1.4	1.3	4	<0.12	0.04	1	>10
	SEST	2−1	4.1	4.0	4	<0.27	0.25	1	>13
V Cyg	OSO	1−0	27.5	27.2	4	2.3	1.9	5	10
	NRAO	2−1	50.1	36.5	2				
	JCMT	2−1	35.9	56.2	7				
	JCMT	3−2	88.9	86.1	7	6.7	8.5	7	12
	JCMT	4−3	123.4	95.2	7				
RV Aqr	SEST	1−0	7.5	6.9	4	0.6	0.6	5	11
	SEST	2−1	18.1	17.2	4				
	SEST	3−2	18.6	20.5	2				
LP And	OSO	1−0	57.0	58.8	2	5.0	5.2	3	10
	IRAM	1−0	92.7	97.4	8				
	NRAO	2−1	60.7	46.5	2				
	JCMT	2−1	90.6	68.5	7	8.7	8.3	7	9
	IRAM	2−1	155.8	166.8	8				
	JCMT	3−2	88.0	79.1	7	10.0	9.6	7	8
	JCMT	4−3	73.3	78.6	7				

1. This paper; 2. Schöier & Olofsson (2000); 3. Schöier & Olofsson (2000, unpublished data); 4. Olofsson et al. (1993a); 5. Olofsson et al. (1993b); 6. Olofsson et al. (1996); 7. JCMT public archive; 8. Neri et al. (1998); 9. Nyman et al. (1993); 10. Ryde et al. (1999).

[a] The observed line ratios have been multiplied by 0.87 to correct for the differences in line strenghts and beam-filling factors (see text for details).

tra obtained by Olofsson et al. (1993a) using the SEST, OSO, and the IRAM 30 m telescope at Pico Veleta, Spain (some of these observations have been remade and the intensities stated in Tab 4 may therefore be somewhat different from those originally given in the reference). Observations of the two lowest rotational transitions have also been performed using the NRAO

12 m telescope at Kitt Peak, USA, and of the J=3→2 line using the SEST (Schöier & Olofsson 2000). In addition, we have obtained publicly available data from the James Clerk Maxwell Telescope (JCMT) at Mauna Kea, Hawaii. The JCMT data are taken at face value. However, in the cases where there are more than one observation available, the derived line intensities are generally consistent within ±20%. In addition, the good agreement with corresponding SEST observations lend further support for the reliability of the JCMT public data.

Thus, for all stars we use data from more than one ^{12}CO transition, in some cases four, to constrain the model. The intensities and overall line shapes of the circumstellar lines produced by the radiative transfer model generally agree well with those observed. This is illustrated here for two of our sample stars CW Leo (Fig. 2) and U Hya (Fig. 3). CW Leo is a high mass loss rate Mira variable where the excitation of ^{12}CO is dominated by collisions. U Hya, on the other hand, is a low mass loss rate object where radiation emitted by the central star plays a role in the excitation. The ^{12}CO model results presented in this paper constitute a sub-sample of the results of an analysis of a large survey of carbon stars presented in Schöier & Olofsson (2000). The reader is referred to this paper for a detailed description of the sensitivity of the model to the various input parameters. However, we point out here that tests made by Schöier & Olofsson show that the derived mass loss rate, for the majority of objects in this study, is mostly affected by the temperature structure and not by the assumed inner radius of the shell or the luminosity of the star, i.e., collisional excitation dominates over radiative excitation. In addition, Schöier & Olofsson have tested the molecular envelope size calculations by comparing radial brightness distributions obtained from the model with those observed. It was found that the envelope sizes estimated using the results from the model by Mamon et al. (1988) are generally consistent with the observations. This is illustrated here in Fig. 2 for CW Leo where the radial brightness distribution of the ^{12}CO(J=1→0) line emission, observed at OSO, is compared to the distribution obtained from the radiative transfer model.

The derived envelope parameters, used as input for the ^{13}CO modelling, are presented in Table 3. We believe that, within the adopted circumstellar model, the estimated mass loss rates are generally accurate to within ±50% (neglecting errors introduced by the uncertain CO abundance and the distance estimates). In the models presented here only ^{12}CO line cooling was included. For the J-stars, cooling from ^{13}CO will be important (scales with the isotope ratio for these low mass loss rate objects), but it will not affect the derived mass loss rate since the heating must be increased, i.e., the kinetic temperature structure will not change significantly, in order to maintain a good fit (Schöier & Olofsson 2000). See also the discussion in Ryde et al. (1999) for the high mass loss rate object IRAS 15194-5115, where radio and far-IR ^{12}CO and ^{13}CO data are modelled.

When comparing our mass loss rate estimate for CW Leo to those obtained from other detailed radiative transfer models (Kastner 1992; Crosas & Menten 1997; Groenewegen et al. 1998) we find a very good agreement, within 20%, when adjustments for differences in f_0 and distance have been made. Kastner (1992) also modelled the high mass loss rate object RW LMi (a.k.a. CIT 6) obtaining (when corrected for the difference in distance) a mass loss rate in excellent agreement with our estimate. Sopka et al. (1989) used a much simpler radiative transfer model to derive the mass loss rate for a number of AGB stars, of which four overlap with our survey. For RW LMi they derived a mass loss rate in excellent agreement with that obtained from our model. For LP And, V384 Per, and V Cyg, however, there are discrepancies of about a factor of two to three. It should be noted though that Sopka et al. (1989) based their mass loss rate estimates on observations of a single line, J=1→0, using a single telescope (OSO). For LP And, the source with the largest discrepancy, we observe a ^{12}CO(J=1→0) line that is almost a factor of two stronger using the same telescope.

4.2. The ^{13}CO modelling

Once the general characteristics of the CSE have been determined from the ^{12}CO analysis, the observed ^{13}CO line emission is modelled. Again, the observed intensities, as well as the line shapes, are generally well reproduced by the model. As for the ^{12}CO modelling, this is illustrated for two of our sample stars, CW Leo (Fig. 2) and U Hya (Fig. 3).

The abundance of ^{13}CO is usually (the J-stars provide an exception) much smaller than that of ^{12}CO, which leads to significantly different excitation conditions for the rarer isotopomer. For instance, the model ^{13}CO line intensities are more sensitive to the assumed properties of the central source of emission, since radiative pumping via the first excited vibrational state becomes important. Indeed, the ^{13}CO J=1→0 and J=2→1 transitions have inverted populations over parts of the envelope even for a high mass loss rate object as CW Leo, Fig. 2. For the high mass loss rate objects, however, the part over which there is a weak maser acting is very small and the emission emanating from this region is not detected in our observations. For thinner envelopes the part of the envelope where the lowest rotational levels are inverted is larger due to the fact that the pumping emission can penetrate further out into the wind. In the case of U Hya, changing the inner radius of the CSE or the luminosity of the star by ∼50% will change the estimated ^{13}CO abundance by ∼20%.

In our modelling of the ^{13}CO line emission we have assumed that the ^{13}CO envelope size is equal to that of ^{12}CO. This is based upon the model results by Mamon et al. (1988). In this model both the effects of photodissociation and of chemical fractionation were included. Chemical fractionation of CO occurs through the exchange reaction (Watson et al. 1976) $^{13}C^+ + ^{12}CO \leftrightarrows {}^{12}C^+ + {}^{13}CO + \Delta E$, where $\Delta E/k$=35 K. Below this temperature, the backward reaction is suppressed and production of ^{13}CO from ^{12}CO is favoured. This reaction can effectively produce ^{13}CO in the outer, cool parts of circumstellar envelopes. Mamon et al. (1988) concluded that the difference between the ^{12}CO and ^{13}CO abundance distributions, when tested over a large mass loss rate interval, is always small, no more than 10 to 20%. Without the effect of chemical fractionation the ^{13}CO envelope would be significantly smaller.

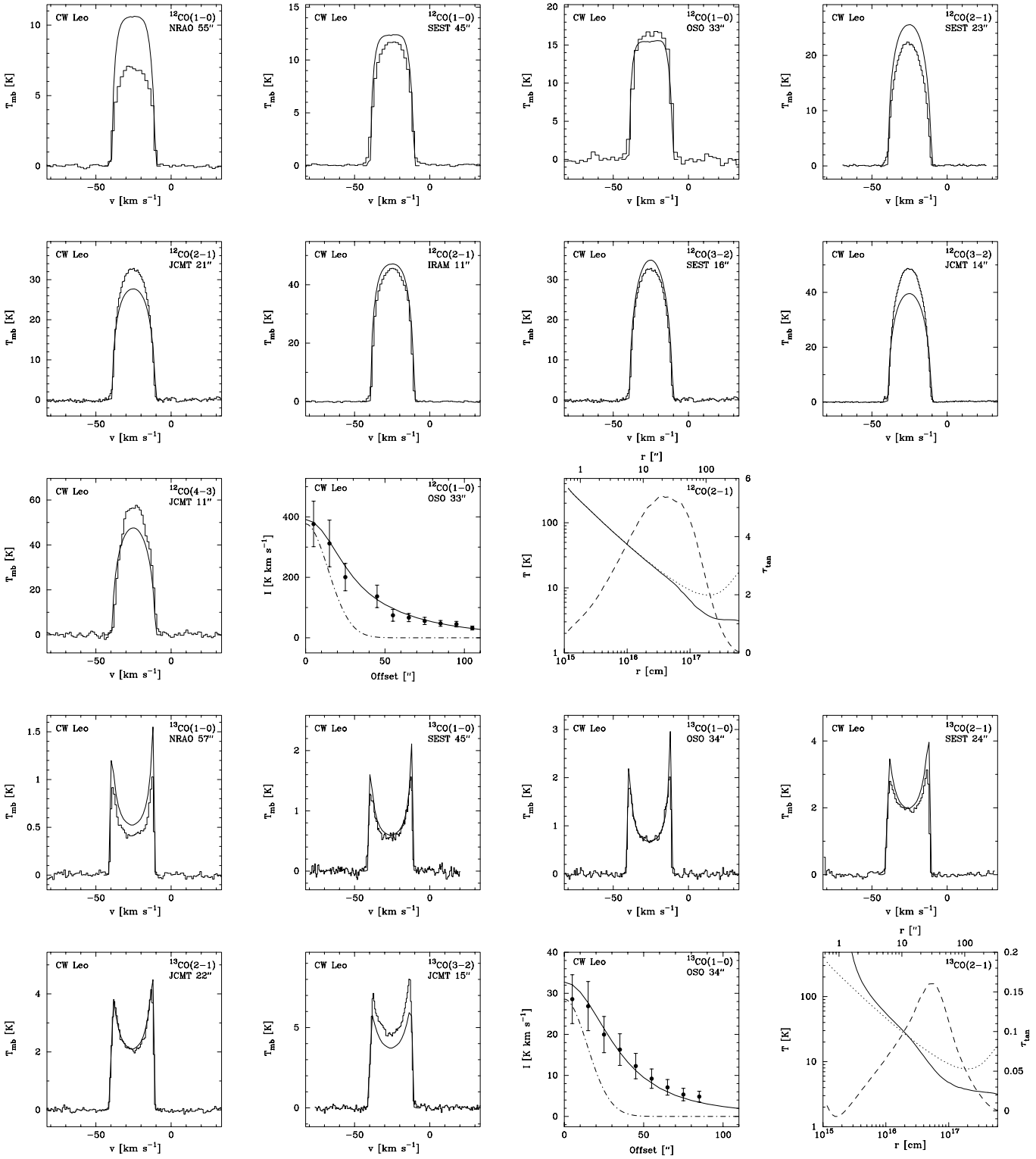

Fig. 2. Multi-transition ^{12}CO and ^{13}CO millimetre wave line emission observed towards the high mass loss rate Mira variable CW Leo. The observed spectra (histograms) have been overlayed with the model prediction (full line) using a mass loss rate of 1.5×10^{-5} M$_\odot$ yr^{-1} and a ^{12}CO/^{13}CO-ratio of 50. The transition, telescope used, and the beamsize, are given for each of the observations. Also shown are the observed radial brightness distributions overlayed by the results from the model (full line). The circular beam used in the radiative transfer is indicated by the dot-dashed line. The full lines in the temperature panels give the excitation temperature of the ^{12}CO(J=2→1) or the ^{13}CO(J=2→1) transition. The dotted lines show the kinetic gas temperature derived from the excitation analysis. The dashed lines give the tangential optical depth, $\tau_{\rm tan}$, of the ^{12}CO(J=2→1) or the ^{13}CO(J=2→1) transition

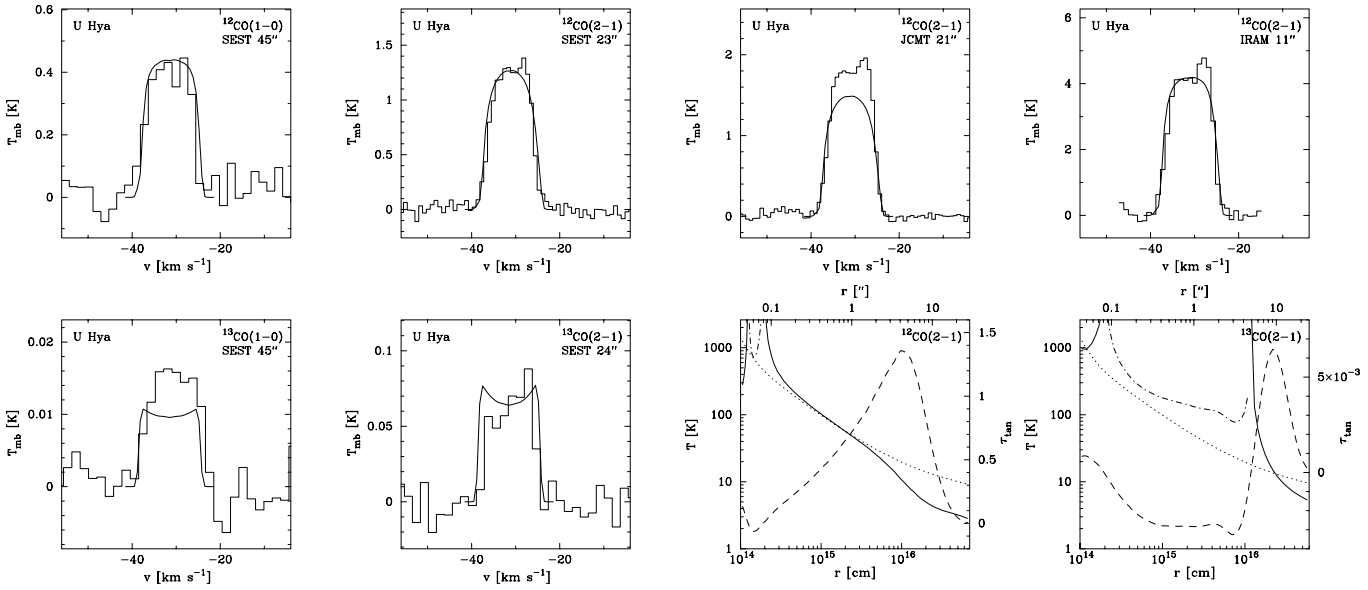

Fig. 3. Multi-transition ^{12}CO and ^{13}CO millimetre wave line emission observed towards the optically bright carbon star U Hya. The observed spectra (histograms) have been overlayed with the model prediction (full line) using a mass loss rate of 1.0×10^{-7} M$_\odot$ yr^{-1} and a ^{12}CO/^{13}CO-ratio of 25. The transition, telescope used, and the beamsize, are given for each of the observations. The full lines in the temperature panels give the excitation temperature of the ^{12}CO(J=2→1) or the ^{13}CO(J=2→1) transition, dash-dot lines indicate a negative excitation temperature, i.e., maser action. The dotted lines show the kinetic gas temperature derived from the excitation analysis. The dashed lines give the tangential optical depth, $\tau_{\rm tan}$, of the ^{12}CO(J=2→1) or the ^{13}CO(J=2→1) transition

This is due to the fact that CO is photodissociated in lines and thereby exhibits considerable self-shielding. Thus, the shielding is higher the higher the optical depth, and hence it is less efficient for the less abundant ^{13}CO. Using OSO we have obtained a brightness distribution map of the ^{13}CO(J=1→0) emission around CW Leo. It is found that the model, with an assumed ^{13}CO envelope size equal to that of ^{12}CO, reproduces the observed radial brightness distribution within the observational errors, Fig. 2. A 20% smaller ^{13}CO envelope gives the same ^{12}CO/^{13}CO-ratio but fails to reproduce the observed radial brightness distribution within the observational errors. This shows the importance of chemical fractionation, at least in the cool outer parts of dense CSEs. In the case of the thin molecular envelope around U Hya a 20% smaller ^{13}CO envelope size would increase the derived ^{13}CO abundance by about 20%. This illustrates that in the case of a thin CSE the CO molecules are effectively excited to the photodissociation radius, i.e., photodissociation determines the size of the emitting region, whereas in a dense CSE excitation sets the size of the emitting region.

4.3. The circumstellar ^{12}CO/^{13}CO-ratio

In Table 4 we list the observed integrated ^{12}CO/^{13}CO line intensity ratios. They are corrected for the differences in line strengths and beam-filling factors (assuming the sources to be unresolved the combined effect gives a ν^{-3} correction, i.e., the observed ratio is lowered by a factor of 0.87). Although we note that some of our CSEs are resolved, we have nevertheless treated all our sources in the same manner. Here we have chosen to integrate the emission over the entire line in order to achieve better signal-to-noise ratios. For optically thin lines this ratio should provide a first order estimate of the abundance ratio. A narrow velocity interval centered on the systemic velocity, where optical depth effects are smallest, should give somewhat higher line intensity ratios than those presented here. Nine of our sample stars have been detected in the ^{13}CO(J=1→0) and/or the ^{13}CO(J=2→1) line. A simple comparison of the ^{12}CO/^{13}CO line intensity ratios and the ^{12}C/^{13}C-ratios derived by Lambert et al. (1986) shows a tight correlation of the form (in the cases where more than one value is available in Table 4 we have used an average),

$$\frac{I(^{12}\mathrm{CO})}{I(^{13}\mathrm{CO})} = (0.6 \pm 0.2) \times \frac{^{12}\mathrm{C}}{^{13}\mathrm{C}}. \quad (3)$$

Thus, a straightforward use of line intensity ratios would lead to ^{12}C/^{13}C-ratios that, on the average, agree with those of Ohnaka & Tsuji (1996). However, any optical depth effects would lower the observed line intensity ratio.

In Table 3 we present the ^{12}CO/^{13}CO-ratios derived using our radiative transfer code. They span a large range, from 2.5 to 90 (steps of 5 in the ^{12}CO/^{13}CO-ratio was used to find the best fit ^{13}CO model, except for the J-stars where a smaller step-size of 0.5 was used). For most of our observed stars the isotope ratio obtained from the detailed radiative transfer is higher than those estimated from simple line intensity ratios. The discrepancy is fairly small for the objects with thin CSEs, but it increases with the thickness of the CSE ($\sim\dot{M}/v_{\rm e}$) and reaches a factor of six for the high mass loss rate objects, Fig. 4. This reflects that even for low to intermediate mass loss rate objects there are optical depth effects, and a detailed modelling is needed to derive reliable isotope ratios. In Table 3 we present, for each star,

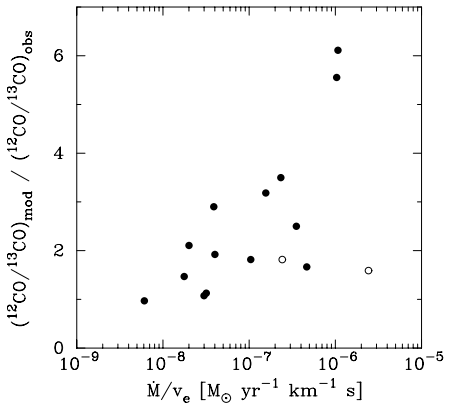

Fig. 4. The ratio between the ^{12}CO/^{13}CO-ratio obtained from the radiative transfer analysis and that obtained from the observed line intensity ratios (in the cases where more than one value is available in Table 4 we have used an average) as a function of the density of the shell ($\sim\dot{M}/v_e$). Sources with detached CSEs are marked as open circles.

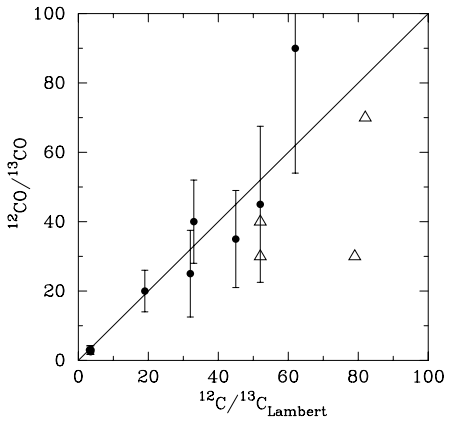

Fig. 5. Comparison between the estimated circumstellar ^{12}CO/^{13}CO-ratio obtained using our detailed radiative transfer code, and the photospheric ^{12}C/^{13}C-ratio estimated by Lambert et al. (1986). An open triangle indicate a lower limit and the solid line represents a 1:1 correlation. Note that at ^{12}C/^{13}C$\sim$3 there are results for three stars.

the maximum tangential optical depth in the ^{12}CO(J=2$\rightarrow$1) transition obtained in the modelling. The radial variation of the tangential optical depth is shown for the high mass loss rate object CW Leo in Fig. 2 and for the low mass loss rate object U Hya in Fig. 3. The optical depth in the ^{12}CO(J=1$\rightarrow$0) line is significantly lower.

The estimated ^{13}CO abundance depends on the adopted ^{12}CO abundance (assumed to be equal for all stars). We find that to a first approximation it scales with f_0, since a lower (higher) f_0 leads to a higher (lower) mass loss rate to fit the ^{12}CO line intensities and hence a lower (higher) ^{13}CO abundance to fit the ^{13}CO line intensities. This means that to a first approximation the estimated ^{12}CO/^{13}CO-ratios are only very weakly dependant on the adopted ^{12}CO abundance. We have varied some of the other parameters in the model (see above), and conclude that in doing so the derived ^{12}CO/^{13}CO-ratio changes by about 20%. With an additional uncertainty of $\pm$15% in the relative calibration of the ^{12}CO and ^{13}CO data (the relative calibration is usually better than the absolute calibration for any given telescope), we estimate that the ^{12}CO/^{13}CO-ratio is uncertain by about $\pm$30%. In the cases were the ^{12}CO/^{13}CO-ratio estimate relies on observations of just one line the uncertainty may be as high as $\pm$50% depending on the quality of the data.

We compare first our derived ^{12}CO/^{13}CO-ratio for CW Leo with those found by others. Crosas & Menten (1997) derived, using a radiative transfer model similar to ours, an isotope ratio of 50, i.e., the same as we do. Greaves & Holland (1997) found a lower ratio of 32, and also a much lower ratio (24) for LP And, using a simple radiative transfer model. Kahane et al. (1992) found the ^{12}C/^{13}C-ratio to be 44 based on observations of optically thin lines. Kahane et al. (1992) also determined the ^{12}C/^{13}C-ratio for RW LMi obtaining a value of 31, in good agreement with our ^{12}CO/^{13}CO estimate for this object. Sopka et al. (1989) estimated ^{12}CO/^{13}CO-ratios for four of our stars that are all lower than our derived values. This is most probably an effect of the difference in the treatment of the radiative transfer. We also note that Dufour et al. (2000, in prep.), derive somewhat lower ^{12}CO/^{13}CO-ratios for the three J-stars.

For our sample stars we compare the circumstellar ^{12}CO/^{13}CO-ratios obtained from the modelling with the photospheric ^{12}C/^{13}C-ratios estimated by Lambert et al. (1986) in Fig 5. A good correlation of the form

$$\frac{^{12}\mathrm{CO}}{^{13}\mathrm{CO}} = (1.0 \pm 0.2) \times \frac{^{12}\mathrm{C}}{^{13}\mathrm{C}} \quad (4)$$

is obtained. Lambert et al. (1986) give an uncertainty in their estimated ^{12}C/^{13}C-ratios of about $\pm$40%. Included in our sample are stars that have had a drastic change in their mass loss rate. For R Scl and S Sct, stars with known detached CSEs (probably) produced during a period of intense mass loss, we have performed the analysis using the envelope parameters determined by Olofsson et al. (1996). These results are included in Fig 5. We note here that our results suggest that the ^{12}C/^{13}C-ratios in the detached shells (with ages of about 10^3 and 10^4 yr for R Scl and S Sct, respectively) are the same as the present ones in the photospheres.

5. The ^{12}C/^{13}C-ratio

Taken at face values our derived ^{12}CO/^{13}CO-ratios support the ^{12}C/^{13}C-ratios derived by Lambert et al. (1986), Fig 5. However, there are a number of uncertainties in the extrapolation from the circumstellar isotopomer result to the stellar isotope ratio. The properties of the CO molecule suggests that the isotopomer ratio in the gas leaving the star is equal to the isotope ratio. We have based our circumstellar model upon the photodissociation/chemical fractionation results of Mamon et al. (1988), and this has so far proven to give good results in our test cases. Our radiative transfer calculations are detailed and also provide good fits to multi-transition data. We also believe that estimates of isotopomer ratios are far less dependant on the adopted circumstellar model than are individual abundances. The two molecules have essentially the same energy level dia-

grams, the same transition strengths, and the same collisional cross sections, and hence their relative abundances are much less dependant on the adopted model than their absolute abundances (note that for ^{12}CO we actually adopt an abundance). However, one should note that the circumstellar estimates apply to time scales of 10^2 to 10^3 years, but there is no reason to expect that these stars have changed their surface composition over such a short time scale. In conclusion, we believe that our derived $^{12}CO/^{13}CO$-ratios are reliable estimates of the stellar $^{12}C/^{13}C$-ratios. Thus, we support the results obtained by Lambert et al. (1986).

Also for the J-stars, whose origin is uncertain, we estimate $^{12}C/^{13}C$-ratios that are more consistent with those of Lambert et al. (1986) than those of Ohnaka & Tsuji (1999), i.e., ratios that are, at least in principle, possible to obtain within the CNO-cycle. IRAS 15194-5115 also has a low $^{12}C/^{13}C$-ratio, but it differs from the J-stars in the sense that it has a much higher mass loss rate (see also Ryde et al. 1999). This star could be a borderline case with a mass of about 3.5 $M_\odot$, where the CNO-cycle produces a low $^{12}C/^{13}C$-ratio, while the temperature is not high enough to effectively convert ^{12}C to ^{14}N (Ventura et al. 1999).

6. Conclusions

We have determined the $^{12}CO/^{13}CO$-ratio in the molecular envelopes around 20 carbon stars, using a detailed non-LTE radiative transfer code. The $^{12}CO/^{13}CO$-ratios found range from 2.5 to 90, and we believe that these ratios accurately measure the stellar $^{12}C/^{13}C$-ratios.

Due to optical depth effects, present mainly in the ^{12}CO line, we find it necessary to treat in detail the radiative transfer in order to obtain reliable isotopomer ratios. For instance, for the two stars in common, we derive $^{12}CO/^{13}CO$-ratios that are almost a factor of two higher than those of Greaves & Holland (1997) in their study of the evolution of the local interstellar $^{12}C/^{13}C$-ratio.

An important ingredient in the model is the molecular abundance distribution in the CSE. We have here used the results of Mamon et al. (1988) for ^{12}CO and ^{13}CO, and we find that for both molecules these are consistent with the observations, although for ^{13}CO we have only been able to test the results for a high mass loss rate object.

Our estimated $^{12}C/^{13}C$-ratios agree well with those estimated in the photosphere by Lambert et al. (1986). Thus, we do not support the claims by other authors that the isotope ratios derived by Lambert et al. (1986) were too high, by about a factor of two.

Acknowledgements. We are grateful to Dr. F. Kerschbaum for generously providing estimates of some of the input parameters to the CO modelling. We would also like to thank Dr. C. Kahane for valuable comments. Financial support from the Swedish Natural Science Research Council (NFR) is gratefully acknowledged.

References

Abia C., Isern J., 1997, MNRAS 289, L11
Bergman P., Carlström U., Olofsson H., 1993, A&A 268, 685
Boothroyd A.I., Sackmann I.J., Ahern S.C., 1993, ApJ 416, 762
Busso M., Gallino R., Wasserburg G.J., 1999, ARA&A 37, 239
Chandra S., Maheshwari V., Sharma A., 1996, A&AS 117, 557
Crosas M., Menten K.M., 1997, ApJ 483, 913
de Laverny P., Gustafsson B., 1998, A&A 332, 661
de Laverny P., Gustafsson B., 1999, A&A 346, 520
Dominy J.F., Wallerstein G., Suntzeff N.B., 1986, ApJ 300, 325
Flower D.R., Launay J.M., 1985, MNRAS 214, 271
Forestini M., Charbonnel C., 1997, A&AS 123, 241
Greaves J.S., Holland W.S., 1997, A&A 327, 342
Groenewegen M.A.T., Whitelock P.A., 1996, MNRAS 281, 1347
Groenewegen M.A.T., van Der Veen W.E.C.J., Matthews H.E., 1998, A&A 338, 491
Heske A., Te Lintel Hekkert P., Maloney P.R., 1989, A&A 218, L5
Kahane C., Cernicharo J., Gomez-Gonzalez J., Guelin M., 1992, A&A 256, 235
Kahane C., Audinos P., Barnbaum C., Morris M., 1996, A&A 314, 871
Kastner J.H., 1992, ApJ 401, 337
Kerschbaum F., 1999, A&A 351, 627
Knapp G.R., Chang K.M., 1985, ApJ 293, 281
Lambert D.L., Gustafsson B., Eriksson K., Hinkle K.H., 1986, ApJS 62, 373
Mamon G.A., Glassgold A.E., Huggins P.J., 1988, ApJ 328, 797
Neri R., Kahane C., Lucas R., Bujarrabal V., Loup C., 1998, A&AS 130, 1
Nyman L.A., Olofsson H., Johansson L.E.B., et al., 1993, A&A 269, 377
Ohnaka K., Tsuji T., 1996, A&A 310, 933
Ohnaka K., Tsuji T., 1998, A&A 335, 1018
Ohnaka K., Tsuji T., 1999, A&A 345, 233
Ohnaka K., Tsuji T., Aoki W., 2000, A&A 353, 528
Olofsson H., Eriksson K., Gustafsson B., Carlström U., 1993a, ApJS 87, 267
Olofsson H., Eriksson K., Gustafsson B., Carlström U., 1993b, ApJS 87, 305
Olofsson H., Bergman P., Eriksson K., Gustafsson B., 1996, A&A 311, 587
Prantzos N., Aubert O., Audouze J., 1996, A&A 309, 760
Ryde N., Schöier F.L., Olofsson H., 1999, A&A 345, 841
Schöier F.L., 2000, PhD thesis, Stockholm Observatory
Schöier F.L., Olofsson H., 2000, A&A submitted
Smith V.V., Lambert D.L., 1985, ApJ 294, 326
Smith V.V., Lambert D.L., 1990, ApJS 72, 387
Sopka R.J., Olofsson H., Johansson L.E.B., Nguyen Q.-R., Zuckerman B., 1989, A&A 210, 78
Ventura P., D'Antona F., Mazzitelli I., 1999, ApJ 524, L111
Wallerstein G., Knapp G.R., 1998, ARA&A 36, 369
Watson W.D., Anicich V.G., Huntress W.T.J., 1976, ApJ 205, L165